An EXAFS investigation of the Zn environment in K_2ZnCl_4 during solid-to-solid phase transformations

1990 J. Phys.: Condens. Matter 2 8557

(http://iopscience.iop.org/0953-8984/2/43/001)

J. Phys.: Condens. Matter **2** (1990) 8557–8565. Printed in the UK

An EXAFS investigation of the Zn environment in K_2ZnCl_4 during solid-to-solid phase transformations

H L Bhat†§, K J Roberts†‡ and M Sacchi†‖

† Department of Pure and Applied Chemistry, University of Strathclyde, Glasgow G1 1XL, UK

‡ SERC Daresbury Laboratory, Daresbury, Warrington WA4 4AD, UK

Received 18 December 1989, in final form 7 August 1990

Abstract. Extended x-ray absorption fine structure (EXAFS) spectroscopy is applied to an investigation of the structural environment around Zn in polycrystalline K_2ZnCl_4 over the temperature range associated with its solid-to-solid phase transformations at 127 °C and 282 °C. The results show a reversible increase in thermal disorder and in the tetrahedral distortion of the $ZnCl_4^{2-}$ anion upon transformation into the incommensurate phase.

1. Introduction

Potassium tetrachlorozincate (K_2ZnCl_4, hereinafter referred to as KZC) crystallizes with a polar orthorhombic structure $Pna2_1$ with $a = 26.86$ Å, $b = 12.47$ Å and $c = 7.28$ Å (Mikhail and Peters 1979). The structure, which is typical of many compounds of the A_2BX_4 (β-K_2SO_4 structure) type, is ferroelectric (Gesi 1978) and commensurate with a wave vector $\boldsymbol{q} = \boldsymbol{a}^*/3$. The structural modulation gives rise to 4 asymmetric units each containing 3 formula units and hence a total of 12 molecules in the unit cell. Phase transitions in this material have been investigated by several workers (Gesi 1978, Gesi and Iizumi 1979, Klug and Sears 1945, Jacobi 1972, Itoh *et al* 1980, Milia *et al* 1983, Quilichini *et al* 1982, Kucharczyk *et al* 1982) and well defined transitions are known to take place at temperatures close to 127 °C and 282 °C. Above the lock-in transition at $\simeq$127 °C the structure is incommensurately modulated along the pseudo-hexagonal a-axis with a wave-vector $\boldsymbol{q} = \frac{1}{3}(1 - \delta)\boldsymbol{q}^*$, where the deviation parameter δ increases with temperature (Kucharczyk *et al* 1982) until close to 284 °C at which the structure transforms to a paraelectric phase with the space group *Pnam*.

The environment around the Zn atoms in the room temperature structure forms a distorted tetrahedron (Mikhail and Peters 1979) where the Zn–Cl distances range from 2.241 to 2.289 Å. There are no structural data currently in the literature concerning how this distortion changes with temperature and how this relates to the phase transformations. In this paper, we describe a preliminary study of structural changes around the Zn atoms in the KZC structure associated with the 127 °C and 282 °C phase transitions using extended x-ray absorption fine structure (EXAFS) spectroscopy.

§ Permanent address: Department of Physics, Indian Institute of Science, Bangalore, India.

‖ Permanent address: LURE, Centre Universitaire Paris-Sud, F-91405 Orsay, France.

0953-8984/90/438557 + 09 $03.50

EXAFS refers to the modulation in the absorption coefficient on the high energy side of an atomic absorption edge as measured in the condensed state (Hayes and Boyce 1982, Lee *et al* 1981, Hastings 1981). The photo-ionization of a core level produces an outgoing electron wave, which is partially back-scattered by the potential of the surrounding atoms. The presence of this incoming component and its interference with the outgoing wave alter the final state configuration for the absorption transition, and in turn the absorption coefficient μ. The normalized EXAFS function is given by

$$\chi(E) = (\mu - \mu_0)/\mu_0 \tag{1}$$

where μ_0 is the smooth background term. The generally accepted formalism for EXAFS treats it as a simple sum of sinusoidal waves, each arising from the various neighbouring shells within the structure. In the plane-wave approximation, we have

$$\chi(k) = -\sum_i [(N_i/kR_i^2)F_i(k)S_0^2(k)\exp(-R_i/\chi(k))\exp(-2k^2A)\sin(2kR_i + \varphi_i)] \tag{2}$$

where R_i is the distance from the absorbing atom to shell i; $\varphi_i(k)$ is the total phaseshift experienced by the photoelectron; $F_i(k)$ is the backscattering amplitude of the neighbouring atoms; N_i is the coordination number of the ith shell; $S_0^2(k)$ and $\exp(-R_i/\chi(k))$ are damping terms and $\exp(-2k^2A)$ is a 'Debye–Waller' type term. In the latter expression A describes structural and thermal disorder and represents the mean square average of the difference in atomic displacements. The photoelectron wavenumber k is given by

$$k = [(2m/h^2)(E - E_{\text{edge}} + E_0)]^{1/2} \tag{3}$$

where E_{edge} is the energy position of the absorption edge threshold and E_0 (typically $\simeq$ 10–20 eV) is an energy offset which represents the difference between the mean potential energy of the solid and that of the lowest unoccupied energy level in the conduction band.

From equation (2), the comparison between experimental and theoretical EXAFS spectra yields information on central atom—nearest neighbour bond lengths (R), and chemical types, through the phaseshifts terms, and on the coordination numbers (N) and disorder (A) through the amplitude terms. By tuning the x-ray photon energy to that of a particular absorption edge, the local arrangement about each type of atom can be determined separately. It is also important to note that long-range order is not required for this technique which makes it, potentially, ideal for investigating structural order in incommensurate solids.

A high intensity, wide bandwidth source of photons, as produced by a synchrotron radiation source, is ideal for measuring EXAFS spectra.

2. Experimental details

Polycrystalline KZC was prepared by recrystallization from 2:1 molar ratio of KCl and $ZnCl_2$. The powdered sample was mixed with boron nitride and pressed into homogeneous pellets about 1 mm thick such that the product of the absorption coefficient and sample thickness was about 2. For some test experiments highly perfect single crystals were also investigated, the growth of which is described elsewhere (El Korashy 1988).

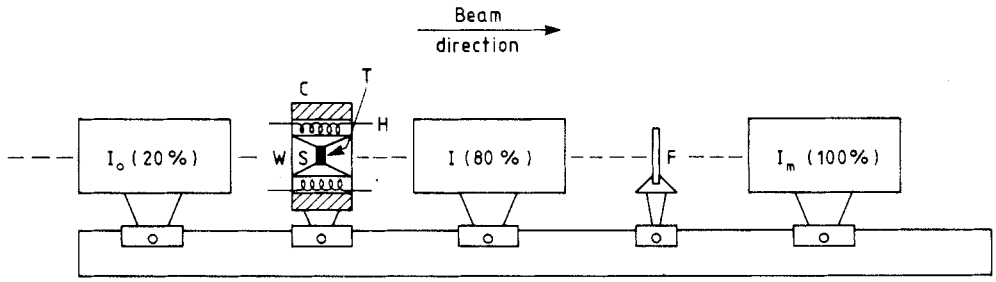

Figure 1. Schematic representation of the experimental set-up. Key: W—kapton window, C—ceramic insulator, H—heating element, S—sample, T—thermocouple, F—Zn calibration foil; I_0, I and I_m are respectively the incident, transmitted and monitor calibration ion chambers, the values in parentheses are the relative absorption factors for the chambers.

The samples were mounted in a compact furnace (Bhat *et al* 1989a) and transmission EXAFS spectra recorded as a function of temperature using station 7.1 of the synchrotron radiation source at SERC Daresbury Laboratory. A Si(111) double crystal monochromator provided an instrumental energy resolution of about 1 eV at the Zn K edge. A zinc metal foil was employed as a monitor for a constant calibration of the energy scale. The experimental set-up is shown in figure 1.

3. Results and discussion

The experimentally recorded absorption spectra ($\mu(E)$) were normalized and background subtracted using the standard data reduction program available at Daresbury. E_0 was defined as the energy at half the maximum step, corrected for the presence of a white line. The pre-edge background, determined by a polynomial interpolation, was subtracted from the whole spectrum. The atom-like smooth contribution ($\mu_0(E)$) to the post-edge absorption was reproduced by spline polynomial functions.

EXAFS spectra were analysed using EXCURV90 (see, for example, Gurman 1988), a program for multi-shell fitting based on curved wave theory. Phase-shift functions for Zn and Cl were obtained from the Daresbury EXAFS Data Bank. They are calculated by the MUFPOT code (Pantos and Firth 1984) starting from a muffin-tin potential and assuming a 1s core-hole model for the absorbing atom. The phase-shift functions used in this work were refined on zinc fluoride and calcium chloride references. All the spectra have been analysed over the same energy range of about 30–620 eV, corresponding to a wavevector range of about 3.5–13 $Å^{-1}$. Prior to quantitative analysis, a Fourier filtering was performed on the rough spectra in order to eliminate high frequency noise and low frequency oscillations introduced by the background subtraction procedure and by remaining atom-like contributions. First the $\chi(k)$ functions, convoluted with a Gaussian window, were Fourier transformed in real space and then an anti-transformation was operated over the range 0.9–2.6 Å (not corrected for phase shift) which guarantees no alterations in the structures of interest.

The structural parameters were refined ($\chi(k)^{the}$) on the filtered and k^3-weighted experimental ($\chi(k)^{exp}$) spectra. Only the chlorine shells were taken into consideration, K atoms being too light and too distant (>3.7 Å) for a reliable quantitative analysis. The fitted data are summarized in tables 1–3 which contain details of the coordination

Table 1. Single-sheli fit with the coordination number fixed at 4. Mean Zn–Cl bond length in the crystalline phase 2.256 Å. Uncertainties in parentheses.

T (°C)	R (Å)	A (Å^2)	FI
25	2.245 (0.002)	0.0106 (0.0002)	0.568
127	2.245 (0.002)	0.0116 (0.0002)	0.681
169	2.238 (0.002)	0.0127 (0.0002)	0.582
212	2.251 (0.004)	0.0152 (0.0003)	1.233
286	2.238 (0.002)	0.0166 (0.0002)	0.438
318	2.238 (0.002)	0.0171 (0.0002)	0.668
25	2.249 (0.002)	0.0105 (0.0002)	0.681

Table 2. Refined parameters for the two-shell models. Uncertainties are given in parentheses. N_t is the total Zn–Cl coordination number which should be 4. FI_f represents the maximum FI value which makes the addition of the second shell statistically meaningful as evaluated by the method of Joyner *et al* (1987). Uncertainties in parentheses.

T (°C)	N	R (Å)	A (Å^2)	N	R (Å)	A (Å^2)	N_t	FI	FI_f
25	2.0	2.207	0.0067	2.1	2.291	0.0072	4.1	0.468	0.538
	(0.1)	(0.004)	(0.0005)	(0.1)	(0.005)	(0.0005)			
127	2.0	2.203	0.0119	2.0	2.269	0.0078	4.0	0.647	0.647
	(0.2)	(0.010)	(0.0019)	(0.2)	(0.009)	(0.0008)			
169	2.1	2.201	0.0066	2.1	2.301	0.0088	4.2	0.481	0.553
	(0.1)	(0.003)	(0.0005)	(0.1)	(0.004)	(0.0006)			
212	1.4	2.162	0.0091	2.7	2.282	0.0083	4.1	0.901	1.170
	(0.2)	(0.005)	(0.0010)	(0.2)	(0.003)	(0.0007)			
286	1.4	2.176	0.0182	2.7	2.273	0.0131	4.1	0.398	0.416
	(0.2)	(0.014)	(0.0015)	(0.2)	(0.006)	(0.0008)			
318	1.6	2.195	0.0085	2.5	2.297	0.0153	4.1	0.503	0.634
	(0.1)	(0.004)	(0.008)	(0.1)	(0.004)	(0.0008)			
25	2.0	2.212	0.0073	2.0	2.291	0.0071	4.0	0.625	0.647
	(0.2)	(0.007)	(0.0007)	(0.2)	(0.008)	(0.0007)			

numbers N, bond distances R, Debye–Waller factors A and fiting index FI. The latter is given by

$$\mathrm{FI} = \sum_{i}^{n_p} \frac{[(\chi(k_i)^{\mathrm{the}} - \chi(k_i)^{\mathrm{exp}})k_i^3]^2}{n_p} \tag{4}$$

where n_p is the number of experimental points.

The analysed Δk and ΔR ranges ($\simeq 10$ Å^{-1} and 1.7 Å respectively) allow for realistic fitting procedures with up to $\simeq 5$ shells ($N_s < \Delta R\, \Delta K/\pi$, where N_s is the number of analysable shells). Initial fits (table 1) were made by holding the coordination number to 4 and iterating the bond lengths and Debye–Waller factors. From the obtained fitting index FI, the value FI_f has been calculated according to the method of Joyner *et al* (1987). FI_f represents the maximum FI value which makes the addition of a further shell statistically meaningful. These values are compared in table 2 with the fitting indexes

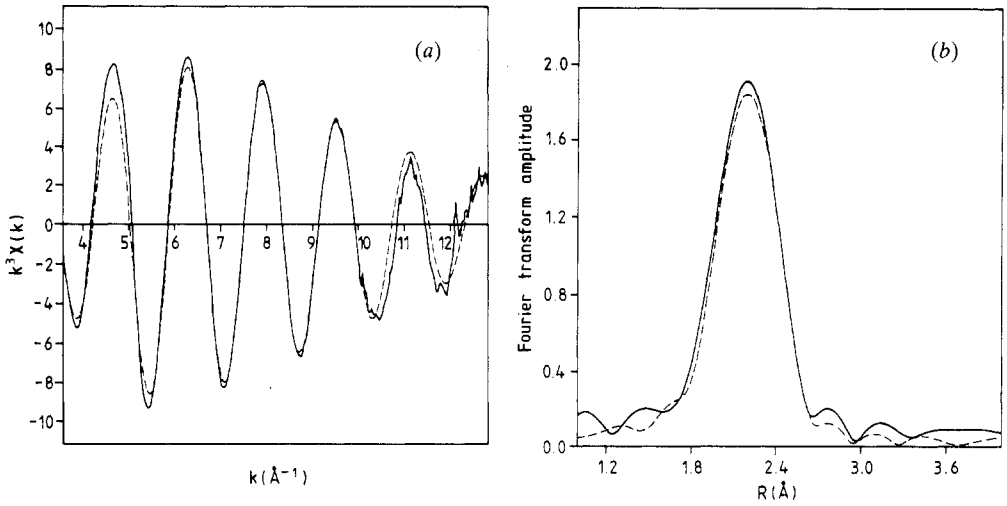

Figure 2. k^3-weighted $\chi(k)$ data taken at 25 °C together with the corresponding Fourier transform. The dashed lines represent the calculated best-fitted curves.

obtained in the two-shell model. In the same table are listed the corresponding structural parameters, which allows a better identification of the nature of the tetrahedral distortion. Figure 2 shows the modelled fits to the k^3-weighted experimental data and their Fourier transforms whilst figure 3 shows how the Fourier transformed data vary as a function of temperature. The expected increase in thermal disorder can be seen in the modelled Debye–Waller factors (table 1) and is clearly noticeable by a reduction in amplitude in the Fourier transforms (figure 3). From the same figure, a slight shift of the maximum towards shorter bond distances can be observed at increasing temperatures. This effect is likely to be related to the thermal motion increase in a similar way to those routinely used for bond length corrections in structural crystallography. The change in tetrahedral distortion as a function of temperature is shown in table 2. Although the radial distribution function (RDF) deduced from the EXAFS data is the summation of the 12 closely distributed Zn–Cl bond lengths, the two-shell model provides a useful insight to the change in the relative weighting of the shells with temperature. Below 212 °C the data can be modelled by 2 shells equally weighted (2:2) at Zn–Cl distances of about 2.20 Å and 2.29 Å whereas above 212 °C the weighting changes to about 1.5:2.5 respectively. It is noteworthy that almost all the fit indices lowered to well below FI_j upon increasing the number of shells to two.

Nonetheless, the data at 212 °C still give a poor fit, and further analysis (table 3) based on a three-shell model suggests a stronger tetrahedral distortion, as evidenced by the Zn–Cl distance at 1.91 Å. Note this effect can be clearly seen in the Fourier transform of figure 3. The degree of reliability of our three-shell model is illustrated in table 4 and figure 5, where the correlation factors for the two- and three-shell fits are reported, as well as relevant correlation maps. As far as the parameters of the added shell are concerned, strong correlation is observed between N and A, mainly due to the uncertainty in A, but not with parameters relating to more distant shells (see figure 5).

Upon recycling to room temperature the structure returns to close to that observed before transformation (figure 4 and table 2). Thus although it is known that these phase

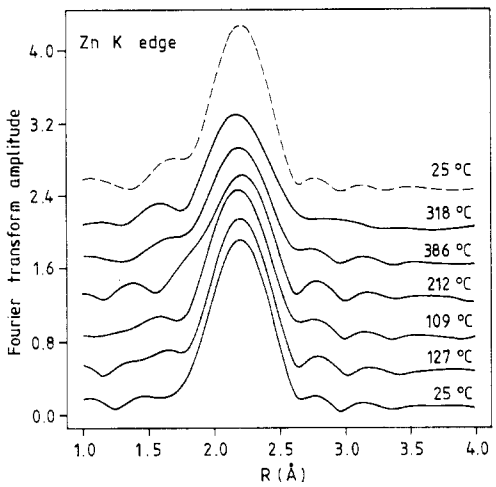

Figure 3. Experimental Fourier transforms as a function of temperature showing the reduction in shell amplitude due to thermal disorder and shift of first-shell maxima to short bond lengths as a function of temperature.

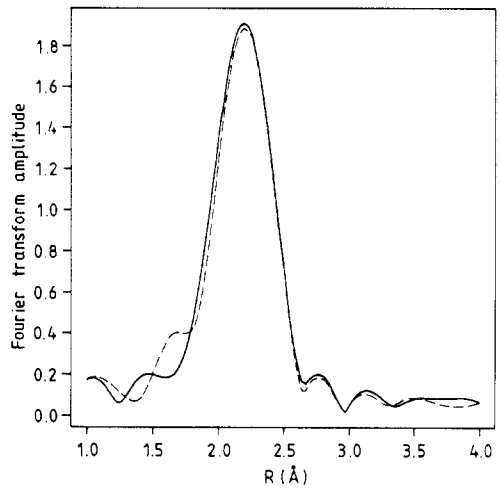

Figure 4. Room temperature Fourier transformed data before (-----) and after (---) thermal cycling showing the reversibility of the structural changes.

Table 3. A three-shell fit to the data taken in the incommensurate phase at 212°C. FI = 0.770 against a required $FI_j = 0.870$. Uncertainties in parentheses.

	N	R (Å)	A (Å^2)
Shell 1	1.4 (0.4)	2.202 (0.031)	0.0140 (0.0024)
Shell 2	2.3 (0.3)	2.276 (0.014)	0.0090 (0.0010)
Shell 3	0.4 (0.1)	1.911 (0.007)	0.0158 (0.0033)

Table 4. Correlation factors between the refined parameters in the two- and three-shell fits for the data taken in the incommensurate phase at 212°C.

	N_1–N_2	N_1–A_1	N_2–A_2	R_1–E_0	R_2–E_0	N_1–N_3	N_2–N_3	N_3–A_3	R_3–E_0
Two-shell	0.647	0.784	0.930	0.822	0.752	—	—	—	—
Three-shell	0.472	0.843	0.837	0.795	0.514	0.023	0.287	0.923	0.477

transformations do induce changes in macro-structure (El Korashy 1988, El Korashy *et al* 1990), we have in this study found no significant evidence correlating such changes to local atomic structure.

A significant disadvantage of EXAFS of powdered samples is that the RDF so obtained does not provide information concerning the asymmetry of the absorber atom site. This disadvantage can be overcome, in principle, using single crystal samples. In such a

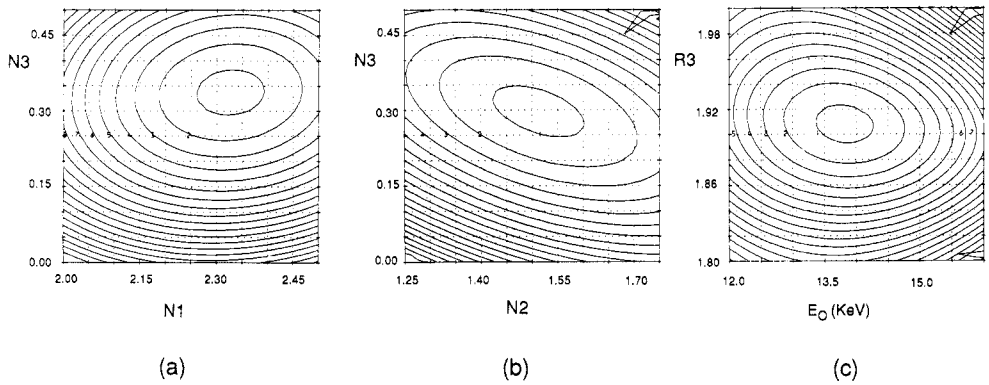

Figure 5. Contour plots obtained using the MAP routine in EXCURVE90 showing the correlation between the structural parameters used in the three-shell fit to the data at $T = 212$ °C. (*a*) N_3 and N_1 (contour increment 0.012), (*b*) N_3 and N_2 (contour increment 0.012), (*c*) R_3 and E_0 (contour increment 0.038).

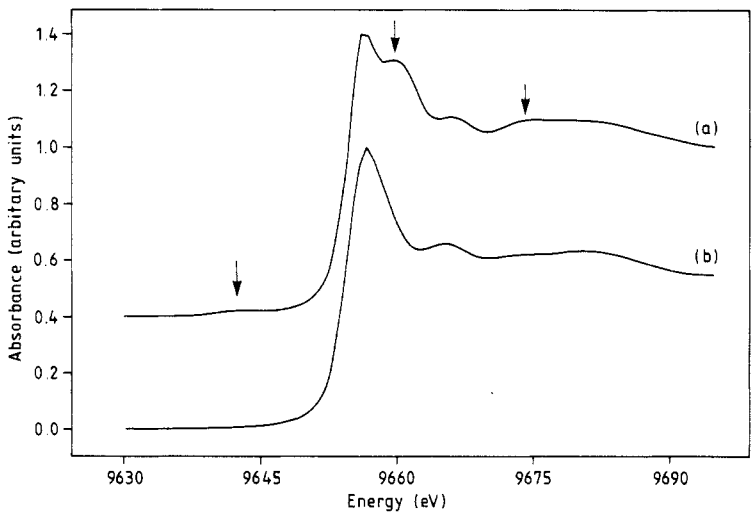

Figure 6. Single-crystal near-edge absorption spectra as a function of crystal orientation: angle between $\boldsymbol{E}$ and [100] equal to 90° (*a*), 0° (*b*). Changes in the near-edge spectra are indicated by the arrows.

measurement the polarization of the synchrotron beam needs to be taken into account as the effective coordination number N for a shell is given (see, e.g., Norman 1986) as

$$N = 3 \sum_j \cos^2 \theta_j \tag{5}$$

where θ_j is the angle between the polarization vector $\bar{\boldsymbol{E}}$ of the synchrotron radiation (in the plane of the storage ring orbit) and the vector $\boldsymbol{R}_j$ from the central atom to the jth atom of the shell. The effect of polarization on the absorption spectra is clearly evident from the near-edge data shown in figure 5.

So far we have not been able to analyse the EXAFS data taken from the single-crystal samples, because of the significant contribution from Laue diffraction in the spectra, particularly in the high-k range (see also Bhat *et al* 1989b). However, it should be possible to overcome this problem with the provision of horizontal and vertical Soller slits after the sample to limit the angular acceptance at the sample. Experiments to test this supposition are currently in hand.

4. Conclusions

This investigation has demonstrated the application of x-ray absorption spectroscopy to studies of the environment around specific atoms in crystalline materials during phase transitions. Studies on KZC show that the tetrahedral distortion changes significantly upon transformation into the incommensurate and the paraelectric phase. Initial studies using single-crystal samples demonstrate the potential of this technique to studies of phase transitions where the probed atom is in a strongly anisotropic crystallographic site. The overall applicability of x-ray absorption spectroscopy to these kind of studies can be summarized as follows.

(i) Where the atoms in a material have absorptions edges in the hard energy (5–30 keV) range then the transmission geometry can be used. Fluorescence yield can also be used where the atom probe is sufficiently dilute ($\simeq 1$ atm%). In this energy range care will be needed to ensure that Laue diffraction effects are eliminated in the case of single crystal samples.

(ii) For materials having atoms with absorption edges in the soft x-ray region (2–5 keV) electron yield or fluorescence yield will need to be considered although this has yet to be put to the test experimentally.

Although lacking in the resolution of conventional crystallography, x-ray absorption spectroscopy provides complementary information in that local rather than long range structural changes can be assessed. Further applications of this technique can be expected, for example:

(i) where the atoms in the crystal have more than one experimentally available absorption edge;

(ii) where the matrix atoms have high back-scattering cross-sections;

(iii) when one wishes to distinguish between two elements on structurally equivalent crystallographic sites which are closely spaced in the periodic table;

(iv) for structurally disordered materials where conventional x-ray crystallographic methods have not proved successful.

The development of quick scanning EXAFS (QEXAFS) techniques (Frahm 1988, Frahm 1989, Edwards *et al* 1990) may mean that structural changes can be mapped-out almost under 'real-time' conditions.

Acknowledgments

We gratefully acknowledge the SERC for the financial support of this work, for the financial support of one of us (HLB) and for the provision of beam time on the Daresbury SRS. We also acknowledge A M Glazer for helpful discussions, A El Korashy who

prepared the single crystals used for the test experiments and the Indian Institute of Science, Bangalore for granting a leave of absence to one of us (HLB).

References

Bhat H L, Clark S M, El Korashy A and Roberts K J 1989a *J. Appl. Crystallogr.* submitted
Bhat H L, Roberts K J and Sacchi X 1989b *Preprint* DL/SCI/661E, SERC Daresbury Laboratory
Edwards B, Garner C D and Roberts K J 1990 *Proc. 2nd Eur. Conf. on X-ray Synchrotron Radiation Research (XSR-89) (Rome, 1989); Nuovo Cimento* at press
El Korashy A 1988 *PhD Thesis* University of Assiut, Egypt
El Korashy A, Klapper H and Roberts K J 1990 in preparation
Frahm R 1988 *Nucl. Instrum. Methods Mater. Res.* A **270** 578
—— 1989 *Physica* B **158** 342
Gesi K 1978 *J. Phys. Soc. Japan* **45** 1431
Gesi K and Iizumi M 1979 *J. Phys. Soc. Japan* **46** 697
Gurman S J 1988 *J. Phys. C: Solid State Phys.* **21** 3699
Hastings J B 1981 *EXAFS Spectroscopy* ed B K Teo and D C Joy (New York: Plenum) p 171
Hayes T M and Boyce J B 1982 *Solid State Physics* vol 37 (New York: Academic) p 173
Itoh K, Kataoka T, Matsunaga H and Nakamura E 1980 *J. Phys. Soc. Japan* **48** 1039
Jacobi H 1972 *Z. Kristallogr.* **135** 467
Joyner R W, Martin K J and Meehan P 1987 *J. Phys. C: Solid State Phys.* **20** 4005
Klug H P and Sears H W 1945 *J. Am. Chem. Soc.* **67** 878
Kucharczyk D, Paciorek W and Kalicinska-Karut J 1982 *Phase Transitions* **2** 277
Lee P A, Citrin P H, Eisenberger P and Kincaid B M 1981 *Rev. Mod. Phys.* **53** 769
Mikhail I and Peters K 1979 *Acta Crystallogr.* B **35** 1200
Milia F, Kind R and Slak J 1983 *Phys. Rev.* B **27** 6662
Norman D 1986 *J. Phys. C: Solid State Phys.* **19** 3273
Pantos E and Firth G D 1984 *EXAFS and Near Edge Structure* vol 3 ed K O Hodgson, B Hedman and J E Penner-Hahn (Berlin: Springer) p 110
Quilichini M, Mathieu J P, Le Postollec M and Toupry N 1982 *J. Physique* **43** 787